ELECTRICAL AND OPTICAL DIAGNOSIS OF A CAVITY HOLLOW-CATHODE POST-DISCHARGE USED AS A SPUTTERING SOURCE

P. C. Balan[a], R. Apetrei[a,b], D. Luca[b], C. Ioniţă[a], R. Schrittwieser[a], G. Popa[b*]

[a]Institute for Ion Physics, University of Innsbruck A-6020 Innsbruck, Austria
[b]Faculty of Physics, "Alexandru Ioan Cuza" University, RO-700506 Iaşi, Romania

Thin films growth using plasma-assisted methods is nowadays a well-established method. The cavity hollow-cathode post-discharge has rapidly become a promising candidate as a sputtering source, due to simplicity of design and operation, good control of parameters and low cost. Additional advantages occur when using the hollow-cathode post-discharge for the sputtering of ferromagnetic materials, where standard magnetrons feature low sputtering rate. We present here experimental results on the electrical and optical diagnosis of a cavity hollow-cathode post-discharge used to deposit Ni thin films. Plasma parameters have been chosen as to cover the operation conditions in real sputtering devices.

1. Introduction

Various techniques of plasma-assisted growth of thin films are being used for applied research and manufacturing, such as dc/rf magnetron and pulsed-laser deposition [1,2]. Specific difficulties are encountered when sputtering ferromagnetic materials owing to the magnetic shielding through the target itself, thus diminishing the sputtering rate. Recently, a simple cavity hollow-cathode post-discharge (CHC-PD)-based sputtering source was proposed [3], which is characterized by high-rate sputtering rate of ferromagnetic materials, as compared with magnetrons. In spite of long-lasting knowledge of CHC-PD, sputtering sources based on it require further characterization.

2. Experimental details

The sputtering source is schematically shown in Fig. 1. In a cylindrical glass tube (1), two 25-mm diameter Ni disks (2) and (3) are used to enclose a 1.4 cm^3 cylindrical cathode cavity (4) within the glass spacer (5). The upper electrode (3) has a central 5 mm diameter cylindrical hole (6) to enhance the ionization rate inside the cathode chamber [4]. A 6 cm diameter ring anode (7) is co-axially inserted 1 cm away from the nozzle, close to the film substrate (located in position 8). Ar gas was introduced in front of the nozzle through three inlets (9, 10), while power was applied to the cathode via the electrode (11). Under normal operation, a conically shaped glowing plasma jet occurs in front of the cathode, where the particle motion is controlled by electrical and pressure gradients.

Electron temperature, electron distribution function (EEDF), and plasma density and potential at the substrate site (2 cm in front of the cathode) were measured using a cylindrical Langmuir probe (tungsten, 0.05 mm in diameter). The ion velocity distribution function (IVDF) in

---

* Corresponding author: ghpopa@uaic.ro

the same region was derived from the *I-V* characteristic of a movable four-grid retarding-field energy analyzer (RFEA). This consisted of four square-shaped planar grids, made of 30 μm diameter stainless steel wires (62% transparency for a mesh size of 150 μm) spaced at 20 μm. The potentials of the grids #1, #2 and # 4 were -15, -53 and -80 V, while the potential of the retarding grid (#3) was swept between -25 and +25 V. IVDFs were computed from the plots of the ion current vs. the potential of the retarding grid, as described elsewhere [5]. The collector was permanently biased at a constant potential of -78 V.
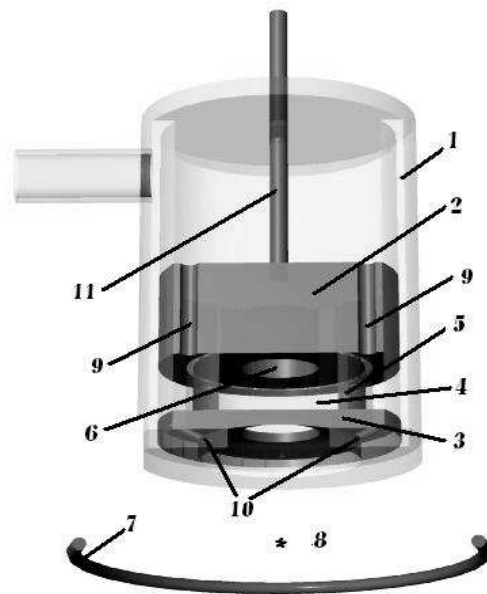
Fig. 1. The schematic diagram of the source.

Optical emissivity measurements (OEM) of the plasma inside the cathode chamber were performed with a view to find the relative variation of plasma density. Low discharge current values were chosen for OEM to keep plasma optically thin and ensure that excitations are due electron-atom collisions and de-excitation by spontaneous transitions, exclusively. Using an optical fiber and a photodiode, the radial distribution of the total light intensity in the range 600 to 850 nm was monitored at different position along the distance between the electrodes (2) and (3). Abel transform applied to the radial distribution of the light intensity was calculated to derive a quantity which is proportional with plasma density.

3. Results and discussion

3.1. Langmuir probe measurements

The visual aspect of the discharge in front of the cathode is shown in Fig. 2. The electrical diagnosis was done under the conditions relevant for sputtering operation, namely for gas pressure ranging between 10×10^{-3} mbar and 100×10^{-3} mbar and 20 to 50 mA, respectively. As demonstrated probe measurements, the electron temperature on the axis of the cathode decreases from around 1 eV in the exit plane of the nozzle to 0.65 eV at 2 cm in front of it, i.e. at the substrate site.

Fig. 2. The visual aspect of the discharge in the sputtering regime.

The variation of the plasma potential and plasma density, as derived from probe measurements are depicted in Fig. 3 for two pressures in the low- and high-range, and a discharge current of 20 mA. Under the low-pressure conditions, plasma potential distribution remains almost constant along the discharge axis. This tendency turns to a monotonous decrease for $p = 70 \times 10^{-3}$ mbar. A similar behavior is evident in the plots of plasma density profiles under the above-mentioned conditions.
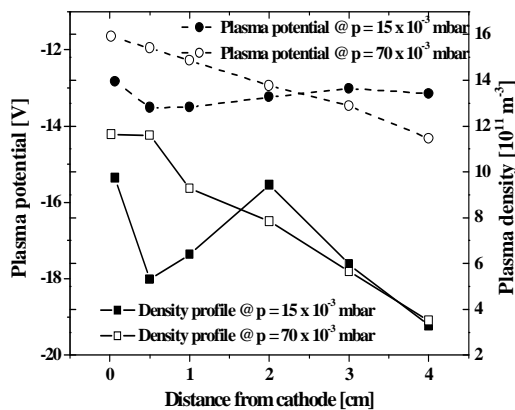
Fig. 3. Axial profiles of plasma potential and density in front of the source.
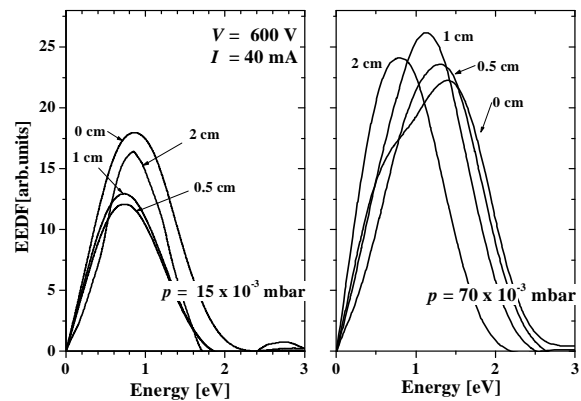
Fig. 4. The electron distribution functions for $p = 15 \times 10^{-3}$ and 70×10^{-3} mbar.

As shown in Fig. 4, the peak value of the EEDF remains practically unchanged over the 2 cm distance in front of the exit nozzle of the cathode under the low-pressure conditions, while it shows a clear tendency to shift towards lower values over the same distance under the pressure values in the high range.

3.2. Retarding-field energy analyzer measurements

The ion velocity distribution was derived from the equation:

$$f(v) = \frac{M_i}{eS}\left(-\frac{dI(E)}{dE}\right) = \frac{M_i}{e^2 S}\left(-\frac{dI(\varphi_r)}{d\varphi_r}\right),$$

(1)

where E and M_i are ion energy and mass, respectively. The value of $f(v)$ was then corrected for the overall transparency of the analyzer. We preferred to express $f(v)$ in the plots shown in Fig. 4 in terms of ion energy (instead of ion velocity), since retarding-field energy analyzer is based on energy discrimination. To convert these values to velocity dependence the equation $v = (2E/M_i)^{1/2}$ should be used. The energy dependences of the ion velocity distribution functions along 4 cm on the discharge axis and for gas pressures ranging between 40×10^{-3} mbar and 80×10^{-3} mbar and a discharge current of 40 mA are depicted in Figs. 5 and 6.
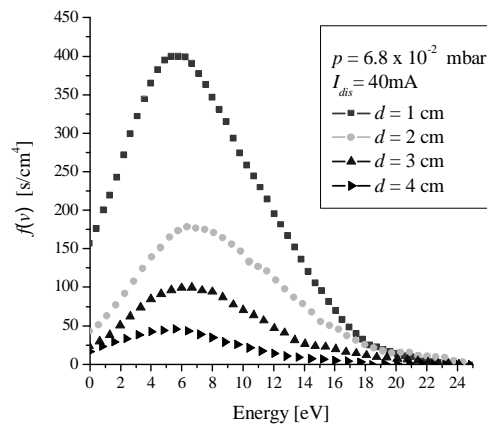
Fig. 5. Ion velocity distribution functions at 1.8 cm in front of the cathode as function of Ar pressure.

The ion velocity distribution function is similar over 4 cm in front of the exit nozzle. It has a peak at approx. 6 eV, irrespective of the distance from the cathode. As for the effect of pressure, which is shown in Fig. 5, there are similar-shapes of the IVDFs taken at a point situated on the axis at 1.8 cm in front of the cathode.

It is worth mentioning that the IVDF tends to narrow and shift towards higher velocities, under lower discharge pressures. The operation in the high-pressure range is affected by significant noise, which is evident in Fig. 6 for the plots corresponding to pressures in excess of 5×10^{-2} mbar.
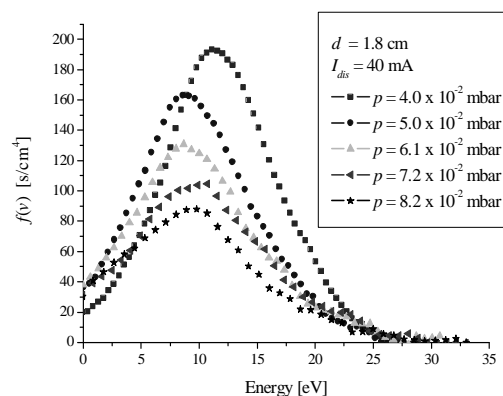
Fig. 6. Ion velocity distribution functions at 1.5 cm in front of the cathode as function of Ar pressure.

3.3. Optical results

As known, in the case of a cylindrical symmetry of the light source, the observed projected intensities can be transformed into radial distribution within the plasma. If $I(y)$ is the experimental intensity of the radiation integrated over the line of sight at a distance y from the centre of the light source and $\varepsilon(r)$ - the local emissivity of the plasma at a distance r from the centre, then $\varepsilon(r)$ *is* related

to $I(y)$ by the Abel inversion relation [6]:

$$\varepsilon(r) = -\frac{1}{\pi}\int_r^R \frac{dI(y)}{dy}\frac{dy}{(y^2-r^2)^{1/2}}$$ (2)

were R is the value of r where $\varepsilon(r)$ becomes zero. The obtained $I(y)$ curves were fitted using a Gaussian function (correlation coefficients $R^2 \cong 0.99$), then used in the Abel inversion to obtain the plasma emissivity, $\varepsilon(r)$.

As shown in Fig. 7, plasma is more confined near the cylindrical hole (6) in the upper electrode of the hollow cathode, while on approaching the lower electrode (3) it expands into the whole cathode cavity (5). This can be explained by the peculiar geometry of the electric field lines between the two electrodes and, therefore, the particularities of the oscillating motion of electrons inside the cathode chamber. This result is well-correlated with the corrosion profile of the higher electrode (Fig. 1) and allows for an optimum shape of the later one for more complicated target geometries, such as composite ones used to prepare compound thin films. SIMION simulations are planned in our lab to find optimum configuration for sputtering.
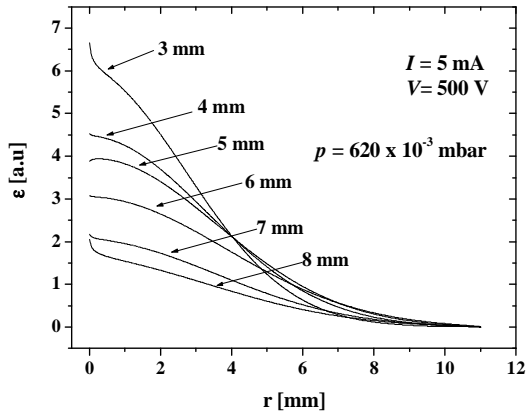
Fig. 7. Plasma emissivity (ε) along the z-axis of symmetry.
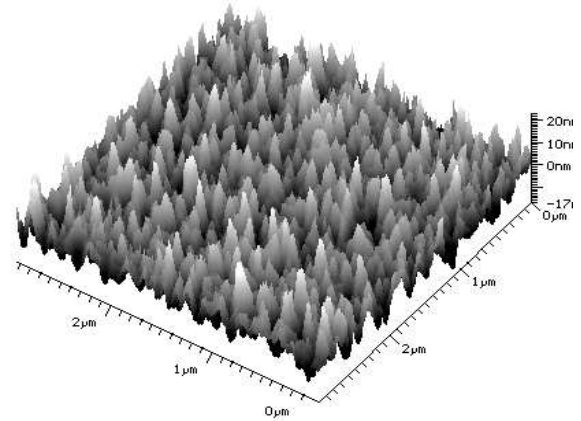
Fig. 8. A typical AFM image of a Ni film surface.

3.4. AFM results

Ni films were deposited at temperatures between RT and 300°C onto glass slides at 2 cm in front of the cathode. The surface morphology was investigated by AFM. Fig. 8 shows a typical image of a 3×3 μm^2 surface of the films deposited under $p = 6\times10^{-2}$ mbar at 300 °C.

To evaluate the surface roughness of our films, the roughness coefficient, R_p, defined by the equation:

$$R_p = \frac{1}{D}\int_0^D |z_0 - z(x)|\, dx$$ (3)

was evaluated over a surface of 3×3 μm^2. Here z_0 is average height over the interval from 0 to D along the x axis. The values of R_p for most of the deposited Ni films were typically around 7.0 nm.

4. Conclusion

Plasma diagnosis was performed to characterize the post-discharge Ar plasma jet in front of the CHC-PD, in the 10^{-2} mbar range. The expansion of the plasma jet in front of the nozzle results in

a rapid decrease of electron temperature, plasma density and ion velocity distribution functions along 2 cm on the cathode axis. Optical measurements showed the highest plasma density inside the cathode cavity occurs in the region of the cylindrical hole in the upper electrode, due to the oscillatory motion of electrons inside the cathode chamber. The actual results suggest that this configuration can be used in the low 10^{-2} mbar range as a sputtering source with beneficial effects of substrate bombardment with energetic particles during deposition and increased ad-atom mobility onto the substrate. Its characteristics allow for preparation of crystal-grade ferromagnetic thin films.

Acknowledgements

References

[1] S. K. Zheng, T. M. Wang, C. Wang, G. Xiang, Nucl. Instr. Method. in Phys. Res.
   B 187, 479 (2002).
[2] L.-S.Hsu, D.Luca, J. Optoelectron . Adv. Mater. **5**, 841 (2003).
[3] M. H. Kazemeini, A. A. Berezin, N. Fukuhara, Thin Solid Films **372**, 70 (2000).
[4] G. Stockhausen, M. Kock, J. Phys. D: Appl. Phys. **34**, 1683 (2001).
[5] C. Böhm, J. Perrin, Rev. Sci. Instrum. **64**, 31 (1993).
[6] W. Lochte-Holtgreven, Plasma Diagnostics, North-Holland, Amsterdam, 1968 p. 184.